optica

Probing, quantifying, and freezing coherence in a thermal ensemble of atoms: supplementary material

ARIF WARSI LASKAR[1], **NIHARIKA SINGH**[1], **PRATIK ADHIKARY**[1], **ARUNABH MUKHERJEE**[1,2], **AND SAIKAT GHOSH**[1,*]

[1]*Department of Physics, Indian Institute of Technology, Kanpur-208016, India*
[1]*Currently at The Institute of Optics, University of Rochester, Rochester, New York 14627, USA*

[*]*Corresponding author:gsaikat@iitk.ac.in*

This document includes the supplementary information for the article "Probing, quantifying and freezing coherence in a thermal ensemble of atoms," https://doi.org/10.1364/optica.5.001462. Here we provide the experimental technique along with theoretical modelling and numerical simulation.

1. EXPERIMENTAL TECHNIQUES

A. Magnetic Field Shielding

Ground state coherence, responsible for electromagnetically induced transparency (EIT), is highly sensitive to external magnetic field. This is used as an advantage for high precision magnetometers. However the presence of a stray magnetic field introduces decoherence in the medium thereby changing the shape and broadening the EIT resonance. Large stray magnetic fields can destroy the resonance completely. Therefore we shield the vapor cell with three layers of μ-metal sheets. The blue curve in Fig. S.1b shows a typical EIT signal obtained by scanning an external magnetic field B in the absence of magnetic shielding. This field is created by sending current through a solenoid with 47 turns placed around the Rb vapor cell. The current is regulated with a feedback control circuit. B introduces a shift of $\mu_B B$ in the atomic energy levels, where μ_B is the Bohr magneton. This shift is opposite for $+$ and $-$ magnetic sub-levels of ground state (Fig. S.1a), thereby changing the two photon detuning as $\delta = \Delta_p - \Delta_c = 2\mu_B B$. The line-width of EIT signal is 93 kHz. The blue curve in Fig. S.1b shows the narrowing of EIT resonance to 30 kHz in the presence of shielding. Another evidence of decoherence introduced by stray magnetic field can be seen in the transient response of the cw probe in the presence of a 10 μs control pulse in Fig. S.1c, where $\delta = 0$. When control is turned off we observe an oscillation of time period 2.45 μs in the probe transmission which corresponds to a magnetic field of 9.5 μT. This indicates population oscillation between states $|1\rangle$ and $|2\rangle$. In the presence of magnetic shielding, this oscillation completely vanishes as seen in Fig. S.1d.

B. Beat note laser locking

Saturation absorption spectroscopy (SAS) is a widely established technique to stabilize the frequency of a laser with respect to an atomic transition. However locking several independent lasers requires independent SAS set-ups, which can be experimentally cumbersome. Another drawback of this technique is that the locked frequency can not be changed arbitrarily. Therefore as a better alternative, we employ a beat note locking technique [1] to stabilize the frequency difference of two independent lasers, one of which is frequency locked. Figure S.2a shows the experimental set up for this technique.

In our experiment scheme (Fig. 1c of the main text), control and probe are derived from an external cavity diode laser (ECDL1, TOPTICA DL pro) which is locked to $|F = 2\rangle \rightarrow |F' = 2, 3\rangle$ crossover by SAS locking technique and later down-shifted by 80 MHz with an AOM. This implies that control and probe are 19 MHz red detuned with respect to $|F = 2\rangle \rightarrow |F' = 1\rangle$ transition. Repumper (ECDL2) and Raman beams (ECDL3) are locked with respect to ECDL1 via beat note lock. In this technique a part of two beams from ECDL1 and ECDL2 (or ECDL3) are mixed on a 50:50 beam splitter, and the beat note signal is recorded on a fast MSM detector (Hamamatsu G4176-03) with a rise time of 30 ps. The beat signal is amplified and then mixed with a reference signal from a VCO (Mini-Circuits ZX95-3360+, $\nu_{VCO} \simeq 3$ GHz). Voltage across VCO is computer controlled using a DAQ card (NI PXIe-6738). The mixer (Mini-Circuits ZX05-C42+) output is split into two equal parts with a power splitter, and a fixed delay is introduced in one part via a longer BNC cable. The two parts are recombined on a phase detector (Mini-Circuits ZAD-1-1+), and the output at their sum frequency is blocked
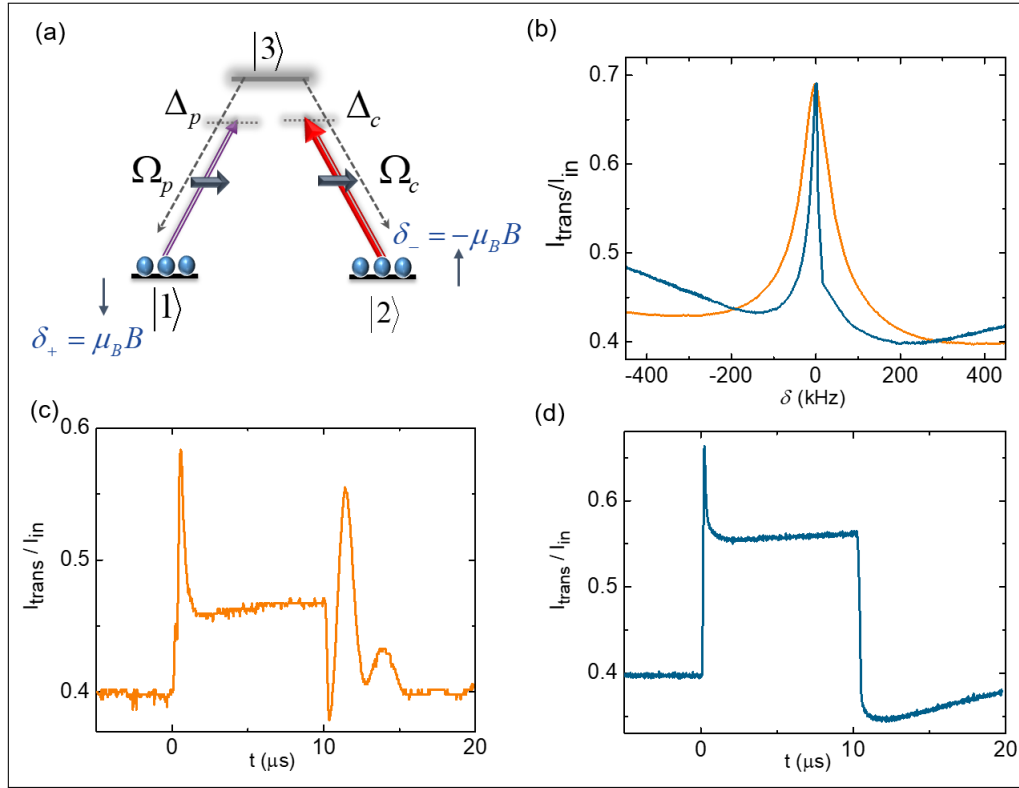
Fig. S.1. Effect of magnetic field shielding. (a) Energy level diagram of Λ system. (b) Steady state probe transmission in the absence (orange) and presence (blue) of magnetic shielding. Frames (c) and (d) show the temporal probe transmission in the absence and presence of magnetic shielding, respectively.
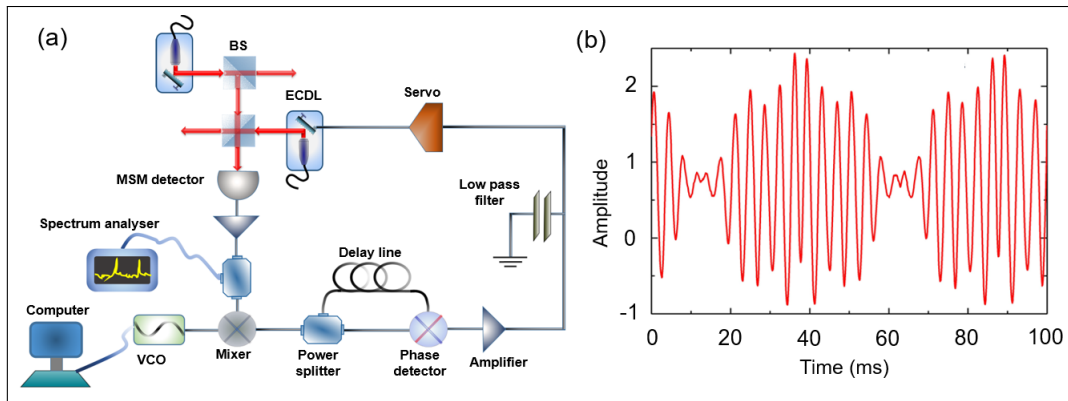

Fig. S.2. Beat note locking. (a) Experimental set up of beat-note lock (b) Beat note fringes.

by a low pass filter. Fig. S.2b shows the output signal of the phase detector while scanning free running laser. Here the time axis corresponds to frequency of the laser. The frequency of free running laser can then be locked with respect to reference laser (ECDL1) using a PID circuit. An added advantage of this robust locking technique is that the frequency of a locked laser can be changed arbitrarily by controlling the VCO frequency. Using this technique repumper is locked at $|F = 3\rangle \longrightarrow |F' = 3\rangle$, while the Raman coherent beams are kept highly red detuned with respect to $|F = 2\rangle \longrightarrow |F' = 1\rangle$ transition where the detuning is controlled by the VCO voltage.

C. Saturation intensity in a Doppler broadened medium

Rabi frequency Ω is related to saturation intensity I_{sat} and natural line-width γ_3 as

$$\frac{I}{I_{sat}} = 2\left(\frac{2\Omega}{\gamma_3}\right)^2 \quad \Rightarrow \quad I_{sat} = \frac{c\epsilon_0 \gamma_3^2 \hbar^2}{4|\hat{e}.d|^2}$$

where $\hat{e}$ is the unit polarization vector, d is the atomic dipole moment, $\Omega = d.\varepsilon_o/2\hbar$ is the resonant Rabi frequency and ε_o is the electric field amplitude [2, 3]. The scattering cross-section in a homogeneously broadened medium is [3]

$$\sigma(\Delta) = \sigma_0 \frac{\gamma_3^2/4}{\gamma_3^2/4 + \Delta^2}, \quad \sigma_0 = \frac{\hbar\omega\gamma_3}{2I_{sat}} \tag{S.1}$$

where σ_0 is the on-resonance scattering cross-section. For a Doppler broadened medium scattering cross-section is Gaussian instead of a Lorentzian,

$$\sigma'(\Delta) = \sigma_D e^{-\Delta^2/\Gamma_D^2} \tag{S.2}$$

where σ_D, Γ_D are the modified on-resonant scattering cross-section and line width due to Doppler broadening. The corresponding change in saturation intensity can be obtained by integrating equations (S.1) and (S.2), which gives

$$\sigma = \int_{-\infty}^{\infty} \sigma(\Delta)d\Delta = \sigma_0\pi\gamma_3, \quad \sigma' = \int_{-\infty}^{\infty} \sigma'(\Delta)d\Delta = \sigma_D\sqrt{\pi/2}\Gamma_D \tag{S.3}$$

Since $\sigma = \sigma'$, using equation (S.1) we have

$$\sigma_D \approx 0.89\frac{\gamma_3}{\Gamma_D}\sigma_0, \quad \sigma_D = \frac{\hbar\omega\gamma_3}{2I_D} \tag{S.4}$$

which finally gives

$$I_D = I_{sat}\frac{\Gamma_D}{0.89\gamma_3} \tag{S.5}$$

where I_D is the saturation intensity for thermal atoms. γ_3, Γ_D and I_{sat} for ^{85}Rb atoms are 6 MHz, 308 MHz and 1.66 mw/cm^2, respectively [2], which gives $I_D \approx 95.75$ mW/cm^2.

2. THEORETICAL MODELLING

A. Density matrix picture

The scheme of Fig. 4a in the main text can be simulated by considering a four level atomic system where the fourth level corresponds to a virtual level which is highly red detuned from the excited state $|3\rangle$. For analytical simplicity the the fourth level can be adiabatically eliminated assuming an effective Raman coupling $\Omega_R = \Omega^+\Omega^- e^{i\phi_R}/\Delta_R$ between the two ground states.

The effective Hamiltonian of the three level system, under dipole and rotating wave approximation, can be expressed as

$$\hat{H} = -(\Delta_p - \Delta_c)|2\rangle\langle 2| - \Delta_p|3\rangle\langle 3| - \Omega_p(z,t)|3\rangle\langle 1| - \Omega_p^*(z,t)|1\rangle\langle 3|$$
$$-\Omega_c(z,t)|3\rangle\langle 2| - \Omega_c^*(z,t)|2\rangle\langle 3| + \Omega_R(z,t)|2\rangle\langle 1| + \Omega_R^*(z,t)|1\rangle\langle 2|. \tag{S.6}$$

Here control and Raman field Rabi frequency are defined as $\Omega_{c,\pm}(z,t) \sim \Omega_{c,\pm}(t) = \Omega_{c,\pm}(0)e^{-(t-t_{on})^2/2\tau^2}$ for $t \leq t_{on}$, $\Omega_{c,\pm}(0)$ for $t_{on} < t < t_{off}$ and $\Omega_{c,\pm}(0)e^{-(t-t_{off})^2/2\tau^2}$ for $t \geq t_{off}$, where τ = 150 ns is the ramp time. The turn-on and turn-off times are $t_{on} = 0$ and $t_{off} = 10$ μs, respectively. The Rabi frequencies are defined as $\Omega_c(0) = d_c \cdot \varepsilon_c(z)/2\hbar$, $\Omega_p(z,0) = d_p \cdot \varepsilon_p(z)/2\hbar$, $\Omega_\pm(0) = d_\pm \cdot \varepsilon_\pm(z)/2\hbar$, with d_c, d_p and $d_\pm$ being the respective transition dipole moments. $\varepsilon_{c,p,\pm}(z)$ are the electric field amplitudes of the corresponding fields. The detunings of these lasers from the corresponding atomic transitions are $\Delta_c = \omega_{32} - \omega_c$, $\Delta_p = \omega_{31} - \omega_p$ and $\Delta_R = \omega_{31} - \omega_- = \omega_{32} - \omega_+$ where ω_p, ω_c and $\omega_\pm$ correspond to the respective carrier frequencies.

Time dynamics of the system is governed by master equation $\dot{\rho}(t) = -i[\hat{H}, \rho] + \hat{L}(\rho)$. Here the first term on the right accounts for coherent interactions while the second term $\hat{L}$ represents irreversible incoherent processes in the system. The evolution of atomic states is therefore given by the following set of equations:

$$\frac{\partial\rho_{11}}{\partial t} = -i\Omega_p\rho_{13} + i\Omega_p^*\rho_{31} + i\Omega_R\rho_{12} - i\Omega_R^*\rho_{21} + \gamma_{31}\rho_{33} - \Gamma_{th}(\rho_{11} - \rho_{11}^{eq}), \tag{S.7}$$

$$\frac{\partial\rho_{22}}{\partial t} = -i\Omega_c\rho_{23} + i\Omega_c^*\rho_{32} - i\Omega_R\rho_{12} + i\Omega_R^*\rho_{21} + \gamma_{32}\rho_{33} - \Gamma_{th}(\rho_{22} - \rho_{22}^{eq}), \tag{S.8}$$

$$\frac{\partial\rho_{33}}{\partial t} = i\Omega_c\rho_{23} - i\Omega_c^*\rho_{32} + i\Omega_p\rho_{13} - i\Omega_p^*\rho_{31} - \gamma_{ex}\rho_{33} - \Gamma_{th}(\rho_{33} - \rho_{33}^{eq}), \tag{S.9}$$

$$\frac{\partial\rho_{12}}{\partial t} = -\Gamma_{12}\rho_{12} + i\Omega_p^*\rho_{32} - i\Omega_c\rho_{13} + i\Omega_R^*(\rho_{11} - \rho_{22}), \tag{S.10}$$

$$\frac{\partial\rho_{13}}{\partial t} = -\Gamma_{13}\rho_{13} - i\Omega_c^*\rho_{12} - i\Omega_R^*\rho_{23} - i\Omega_p^*(\rho_{11} - \rho_{33}), \tag{S.11}$$

$$\frac{\partial\rho_{23}}{\partial t} = -\Gamma_{23}\rho_{23} - i\Omega_p^*\rho_{21} - i\Omega_R\rho_{13} - i\Omega_c^*(\rho_{22} - \rho_{33}), \tag{S.12}$$
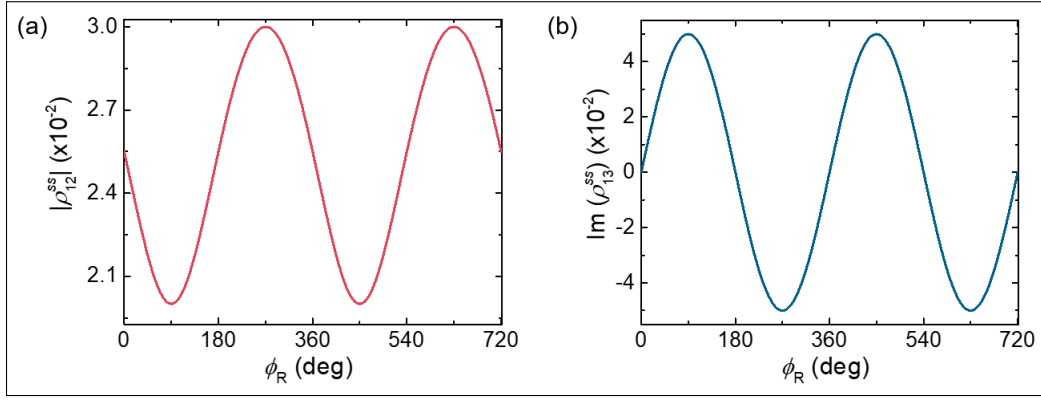
Fig. S.3. Phase dependence of ρ_{12}^{ss} and ρ_{13}^{ss}. (a) $|\rho_{12}^{ss}|$ and (b) $Im(\rho_{13}^{ss})$ as a function of ϕ_R. Here $\Omega_p = 5.0 \times 10^{-3}\gamma_3$, $\Omega_c = 1.0\gamma_3$, $\Omega_R = 2.5 \times 10^{-2}\gamma_3$ and $\gamma_3 = 6.0(2\pi)$ MHz.

where

$$\Gamma_{12} = \Gamma_{decoh} + \Gamma_{th} + i(\Delta_p - \Delta_c), \tag{S.13}$$

$$\Gamma_{13} = \Gamma_{decoh} + \frac{\gamma_{ex}}{2} + \Gamma_{th} + i\Delta_p, \tag{S.14}$$

$$\Gamma_{23} = \Gamma_{decoh} + \frac{\gamma_{ex}}{2} + \Gamma_{th} + i\Delta_c, \tag{S.15}$$

$$\gamma_3 = \gamma_{31} + \gamma_{32}, \quad \gamma_{ex} = \gamma_3 + \gamma_{out}. \tag{S.16}$$

Here γ_{out}, Γ_{decoh} and Γ_{th} are the radiative decay from excited state $|3\rangle$ out of the closed Λ system, decoherence rate and transit time decay, respectively. The steady state solutions for ρ_{12} and ρ_{13} are

$$\rho_{12}^{ss} = [i\Omega_p^*\rho_{32}^{ss} - i\Omega_c\rho_{13}^{ss} + i\Omega_R^*(\rho_{11}^{ss} - \rho_{22}^{ss})]/\Gamma_{12}, \tag{S.17}$$

$$\rho_{13}^{ss} = [-i\Omega_c^*\rho_{12}^{ss} - i\Omega_R^*\rho_{23}^{ss} - i\Omega_p^*(\rho_{11}^{ss} - \rho_{33}^{ss})]/\Gamma_{13}. \tag{S.18}$$

For weak probe field $\Omega_p << \Omega_c, \Omega_R$, analytical solutions for ρ_{ij}^{ss} can be obtained using the perturbation approach as $\rho_{ij} = \rho_{ij}^{(0)} + \rho_{ij}^{(1)}$. The zeroth order solutions are:

$$\rho_{11}^{ss,(0)} \simeq 1, \quad \rho_{22}^{ss,(0)} = \rho_{33}^{ss,(0)} \simeq 0, \tag{S.19}$$

$$\rho_{12}^{ss,(0)} = \frac{i\Omega_R^*}{\Gamma_{12} + \frac{|\Omega_c|^2}{\Gamma_{13}(1+|\Omega_R|^2/\Gamma_{13}^2)}}, \tag{S.20}$$

$$\rho_{13}^{ss,(0)} = \frac{\Omega_c^*\Omega_R^*}{\Gamma_{12}\Gamma_{13}(1 + \frac{|\Omega_R|^2}{\Gamma_{13}^2}) + |\Omega_c|^2} \tag{S.21}$$

where we have assumed that $\Gamma_{13} = \Gamma_{23}$. The above equations represent the contribution of Raman fields to the three level EIT system. First order solutions are

$$\rho_{12}^{ss,(1)} = \frac{-\Omega_c\Omega_p^*[\Gamma_{13}(\Gamma_{13}^*|\Omega_c|^2 + \Gamma_{12}^*\Gamma_{13}^{*2} + \Gamma_{12}^*|\Omega_R|^2) + \Omega_R^2(\Gamma_{13}^2 - \Gamma_{13}^{*2})]}{(\Gamma_{13}^*|\Omega_c|^2 + \Gamma_{12}^*\Gamma_{13}^{*2} + \Gamma_{12}^*|\Omega_R|^2)(\Gamma_{13}|\Omega_c|^2 + \Gamma_{12}\Gamma_{13}^2 + \Gamma_{12}|\Omega_R|^2)}, \tag{S.22}$$

$$\rho_{13}^{ss,(1)} = \frac{-i\Omega_p^*[\Gamma_{13}|\Omega_c|^2(\Gamma_{12}\Gamma_{13}^* - \Omega_R^2) + \Gamma_{12}(\Gamma_{13}^{*2} + |\Omega_R|^2)(\Gamma_{12}^*\Gamma_{13} - \Omega_R^2)]}{(\Gamma_{13}^*|\Omega_c|^2 + \Gamma_{12}^*\Gamma_{13}^{*2} + \Gamma_{12}^*|\Omega_R|^2)(\Gamma_{13}|\Omega_c|^2 + \Gamma_{12}\Gamma_{13}^2 + \Gamma_{12}|\Omega_R|^2)}. \tag{S.23}$$

The above equations comprises of the EIT terms and higher order corrections of Raman fields. When Γ_{12}, Γ_{13} are real, the above equations assume a very simple form:

$$\rho_{12}^{ss,(1)} = \frac{-\Omega_c\Omega_p^*\Gamma_{13}}{\Gamma_{13}|\Omega_c|^2 + \Gamma_{12}\Gamma_{13}^2 + \Gamma_{12}|\Omega_R|^2}, \tag{S.24}$$

$$\rho_{13}^{ss,(1)} = \frac{-i\Omega_p^*(\Gamma_{12}\Gamma_{13} - \Omega_R^2)}{\Gamma_{13}|\Omega_c|^2 + \Gamma_{12}\Gamma_{13}^2 + \Gamma_{12}|\Omega_R|^2} \tag{S.25}$$

which are the usual EIT terms in absence of Ω_R.

The time dependent response of the medium is obtained by numerically integrating the density matrix equations along with Maxwell wave propagation equation

$$\frac{1}{c}\frac{\partial\Omega_p}{\partial t} + \frac{\partial\Omega_p}{\partial z} = -i\mu_a\rho_{13}(z,t). \tag{S.26}$$

Here $\mu_a = Nd_p^2\omega_p/\hbar\epsilon_0$ where c and ϵ_0 correspond to speed of light and dielectric susceptibility in vacuum, respectively. The transmitted probe pulse is $\Omega_p(t + \tau) = \Omega_p(t) + \int_0^L \alpha Im(\rho_{13}(z,t))dz$, where L is the propagation length in the cell and α is a constant [4].

B. Wave function picture

The evolution of probability amplitudes corresponding to Hamiltonian in equation (S.6) can be written as

$$\dot{C}_1 = i\Omega_p^*C_3 - i\Omega_R^*C_2 - i\frac{\Omega_-^2}{\Delta_R^2}\gamma_3 C_1, \tag{S.27}$$

$$\dot{C}_2 = -(\frac{\gamma_2}{2} - i(\delta + \frac{\Omega_+^2}{\Delta_R^2}\gamma_3))C_2 + i\Omega_c^*C_3 - i\Omega_R C_1, \tag{S.28}$$

$$\dot{C}_3 = -(\frac{\gamma_3}{2} - i\Delta_p)C_3 + i\Omega_p C_1 + i\Omega_c C_2 \tag{S.29}$$
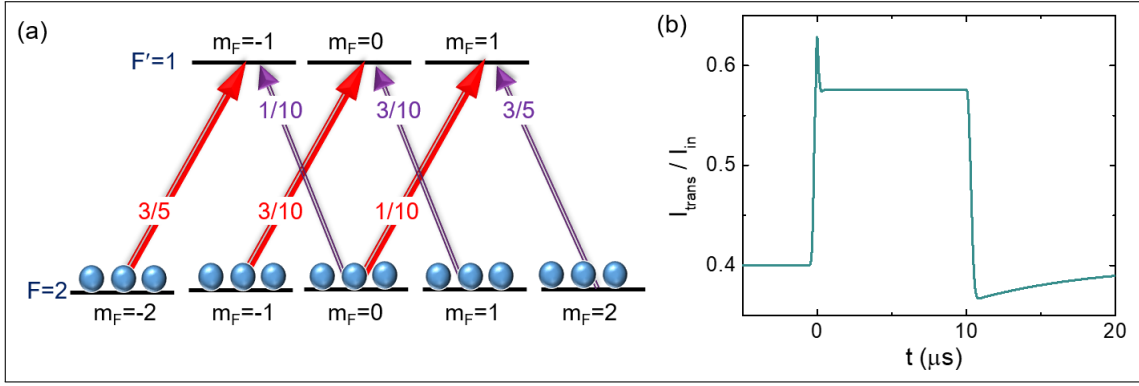
Fig. S.4. Coupled Λ systems within the Zeeman manifold. (a) Atomic energy level scheme for complete Zeeman manifold of ^{85}Rb D_2 $|F = 2\rangle \to |F' = 1\rangle$ transition. The red and purple arrows represent the control and probe field couplings, respectively. The numbers on these lines represent the respective transition strengths. (b) Numerically simulated probe transmission for closed 8-level system.

where γ_2 is decay rate of $|2\rangle$. For $C_1 \simeq 1$, the steady state solutions are

$$C_2\widetilde{\Gamma}_2 = i\Omega_c^* C_3 - i\Omega_R, \tag{S.30}$$

$$C_3\Gamma_3 = i\Omega_p + i\Omega_c C_2 \tag{S.31}$$

where $\widetilde{\Gamma}_2 = \frac{\gamma_2}{2} - i(\delta + \frac{\Omega_+^2}{\Delta_R^2}\gamma_3)$ and $\Gamma_3 = \frac{\gamma_3}{2} - i\Delta_p$. Substituting the value of C_2 in equation(S.31) we get

$$C_3 = \frac{i\Omega_p}{\Gamma_3} + \frac{i\Omega_c}{\Gamma_3}\left(\frac{i\Omega_c^*}{\widetilde{\Gamma}_2}C_3 - \frac{i\Omega_R}{\widetilde{\Gamma}_2}\right),$$

which implies

$$C_3 = \frac{\widetilde{\Gamma}_2}{\widetilde{\Gamma}_2\Gamma_3 + |\Omega_c|^2}\left[i\Omega_p + \frac{\Omega_R\Omega_c}{\widetilde{\Gamma}_2}\right]. \tag{S.32}$$

Substituting C_3 in equation(S.30) we have

$$C_2 = \frac{-\Omega_c^*\Omega_p}{\widetilde{\Gamma}_2\Gamma_3 + |\Omega_c|^2} - \frac{i\Omega_R}{\widetilde{\Gamma}_2}\left[1 - \frac{|\Omega_c|^2}{\widetilde{\Gamma}_2\Gamma_3 + |\Omega_c|^2}\right], \tag{S.33}$$

which means

$$\rho_{21}^{ss} = \frac{-\Omega_c^*\Omega_p}{\widetilde{\Gamma}_2\Gamma_3 + |\Omega_c|^2} - \frac{i\Omega_R}{\widetilde{\Gamma}_2}\left[1 - \frac{|\Omega_c|^2}{\widetilde{\Gamma}_2\Gamma_3 + |\Omega_c|^2}\right], \tag{S.34}$$

$$\rho_{31}^{ss} = \frac{i\Omega_p\widetilde{\Gamma}_2}{\widetilde{\Gamma}_2\Gamma_3 + |\Omega_c|^2} + \frac{\Omega_R\Omega_c}{\widetilde{\Gamma}_2\Gamma_3 + |\Omega_c|^2}. \tag{S.35}$$

For $\Omega_c \gg \Omega_p, \Gamma_3, \widetilde{\Gamma}_2$

$$\rho_{21}^{ss} = -\frac{\Omega_c^*\Omega_p}{|\Omega_c|^2} - \frac{i\Omega_R\Gamma_3}{|\Omega_c|^2}$$

$$= -\frac{|\Omega_p|}{|\Omega_c|}e^{i\phi_0} - \frac{|\Omega_R|}{|\Omega_c|^2}|\Gamma_3|e^{i(\phi_R + \phi_3 + \pi/2)}$$

$$= e^{i\phi_0}[A + Be^{i(\phi_R + \phi_3 + \pi/2 - \phi_0)}], \tag{S.36}$$

where $\phi_0 = \phi_p - \phi_c$ is the relative phase between control and probe fields, ϕ_R is the phase between Raman beams, $\Gamma_3 = |\Gamma_3|e^{i\phi_3}$ and $A = -\frac{|\Omega_p|}{|\Omega_c|}$ and $B = -\frac{|\Omega_R|}{|\Omega_c|^2}|\Gamma_3|$. The absolute value of ρ_{21}^{ss} is therefore given as

$$|\rho_{21}^{ss}| = \sqrt{A^2 + B^2 + 2AB\cos(\phi_R - \phi_0 + \phi_3 + \pi/2)}, \tag{S.37}$$

and

$$\rho_{31}^{ss} = \frac{i\Omega_p\widetilde{\Gamma}_2}{|\Omega_c|^2} + \frac{\Omega_R\Omega_c}{|\Omega_c|^2}. \tag{S.38}$$

Since susceptibility $\chi \propto \rho_{31}/\Omega_p$, in the limit of $\gamma_2 = 0$ we have

$$\frac{\rho_{31}^{ss}}{\Omega_p} = \frac{\delta'}{|\Omega_c|^2} + \frac{|\Omega_R||\Omega_c|}{|\Omega_c|^2|\Omega_p|}e^{i(\phi_R - (\phi_p - \phi_c))}$$

$$= \frac{\delta'}{|\Omega_c|^2} + \frac{|\Omega_R|}{|\Omega_c||\Omega_p|}e^{i(\phi_R - \phi_0)}, \tag{S.39}$$

where $\delta' = \delta + \frac{\Omega_+^2}{\Delta^2}\gamma_3$. Figure S.3 shows the dependence of phase ϕ_R on ρ_{12}^{ss} and ρ_{13}^{ss}. From equation (S.39) we have

$$Re(\frac{\rho_{31}^{ss}}{\Omega_p}) = \frac{\delta'}{|\Omega_c|^2} + \frac{|\Omega_R|}{|\Omega_c||\Omega_p|}cos(\phi_R - \phi_0), \tag{S.40}$$

$$Im(\frac{\rho_{31}^{ss}}{\Omega_p}) = \frac{|\Omega_R|}{|\Omega_c||\Omega_p|}sin(\phi_R - \phi_0), \tag{S.41}$$

which implies

$$tan(\phi_{eff}) = \frac{\frac{|\Omega_R|}{|\Omega_c||\Omega_p|}sin(\phi_R - \phi_0)}{\frac{\delta'}{|\Omega_c|^2} + \frac{|\Omega_R|}{|\Omega_c||\Omega_p|}cos(\phi_R - \phi_0)}. \tag{S.42}$$

C. Numerical simulations for the complete Zeeman manifold

Though the numerical simulation of a simple three level model agrees well with our experiments, in reality there are other levels in the Zeeman manifold which makes the system very complicated. The coherent dynamics in such systems is essentially dominated by the formation of a dark state. It was first observed by Parkins et.al. [5] that even for a multilevel atom, with a ground state Zeeman structure, there is always formation of similar dark states in presence of circularly polarized control and probe fields. Subsequently, such dark states, formed effectively between the stretched states for multilevel systems have been used explicitly for various schemes [6, 7]. Eventually, experiments on such multilevel atoms also started using and effective three-level model to simulate observations [8, 9]. We follow this approach, relying on the fact that the simplicity and power of a three-level model can elucidate most of the essential features of a coherent dark state dynamics.
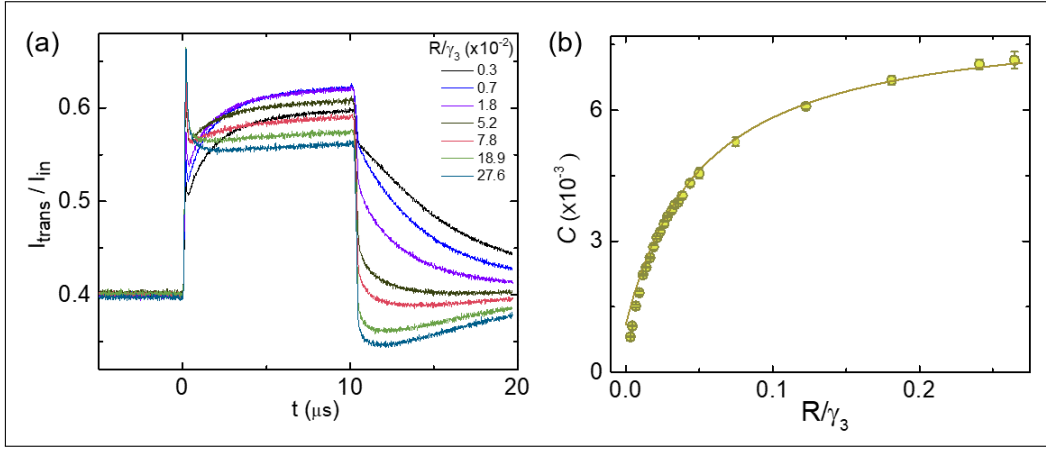
Fig. S.5. Evidence of additivity. (a) Probe transmission for varying repumper rates R. Here $\Omega_c = 2.3 \times 10^{-1}\gamma_3$. (b) Extracted coherence (circles) as a function of repumper rate. Solid line shows the simulated $|\rho_{12}|$.

However, for the sake of completeness we consider the complete Zeeman manifold of ^{85}Rb D_2 $|F = 2\rangle \to |F' = 1\rangle$ transition as shown in Fig. S.4a. This system comprises of three mutually coupled Λ system and its evolution is governed by 36 coupled equations. We solve the density matrix equations and propagate the field with Maxwell equation (S.26) similar to the case of three level system. Figure S.4b shows the simulated probe transmission for closed eight level scheme which is similar to the response obtained by simulating a three level Λ system, thereby validating the fact that a simplified three-level scheme captures most of the essential features for a complicated multi-level system.

3. SOME COMMENTS ON EXPERIMENTAL RESULTS

A. Coherence quantification vs measure, in an experimentally simulated closed system

The presence of neighbouring levels make it impossible to experimentally realize a closed three level system as shown in Fig. S.1a. To counter the leakage of atoms outside the Λ manifold, we use an incoherent repumper field which pumps the scattered atoms back to the system, thereby effectively closing the system. By tuning the repumper intensity we can change the system from closed to open. This can be verified in Fig. S.5a, where it is seen that as the repumper intensity decreases, the fall height $\Delta h = h1 - h2$ decreases making the system more and more incoherent (open).

We have defined coherence quantifier C in terms of Δh (section III of main text). For a quantity to qualify as a measure of coherence, it needs to satisfy the following conditions [10]: (1) the quantifier should be positive, (2) it should not increase under incoherent operation, (3) it should be monotonic, (4) it should be an additive quantity. We find that C indeed satisfies all these conditions. As C is proportional to Δh, the condition $\Delta h_{closed} > \Delta h_{open} > \Delta h_{incoherent}$ implies

$$C_{closed} > C_{open} > C_{incoherent}, \tag{S.43}$$

which also proves that C cannot be negative because the minimum bound of C is given by $\Delta h_{incoherent} = 0$. Further equation (S.43) implies that C decreases under incoherent operation. Monotonicity of C can be verified from Figure S.5b, where it is observed that as the repumper intensity increases, i.e., as the system gets more and more closed (coherent), C also increases.

Numerical results show an excellent agreement with the experiment as shown by solid line in Fig. S.5b. Additivity of C can be established from the linear region of Fig. S.5b (R/$\gamma_3 \simeq$ 0 - 0.07), where it is clear that C is linearly proportional to number of atoms in the closed Λ system.

B. Signature of EIT to ATS transition in ρ_{21}

The EIT to ATS transition shown in Fig. 3 of the main text is not captured in the probe transmission, but is clearly visible in C i.e $|\rho_{21}|$. This can be explained in terms of ρ_{21}^{ss} as given by equation (S.34) (for $\Omega_R = 0$)

$$\rho_{21}^{ss} = \frac{-\Omega_c^* \Omega_p}{\Gamma_2 \Gamma_3 + |\Omega_c|^2}, \tag{S.44}$$

where $\Gamma_2 = \gamma_2/2 - i\delta$ and $\Gamma_3 = \gamma_3/2 - i\Delta_p$. For $\Omega_c << \Gamma_2\Gamma_3$, we can see that there is one pole of $|\rho_{21}^{ss}|$ at $\Delta_p = 0$, while for larger control strength, there are two poles at $\pm\sqrt{2}\Omega_c$, which indicates splitting in $|\rho_{21}^{ss}|$ at large control strengths and agrees with the observations in Fig. 3c of the main text.

C. Offset in C with respect to C^{EIT}

For the phase coherent decay compensation scheme as shown in Fig. 4a of the main text, large detuning Δ_R ensures a build up of two-photon coherence with minimal population reshuffle, simply adding a perturbative correction to the coherence. However the sinusoidal variation of C with ϕ_R is not symmetric with respect to C^{EIT} as may be seen in Fig. S.6a (also in Fig. 4b of the main text). This is indicative of limitation of the perturbative analysis, with Raman fields competing with control in redistributing the populations. Figure S.6b shows the variation of offset in C with respect to C^{EIT} as a function of $|\Omega_-|^2/|\Delta_R|^2$ where we have considered that $\Omega_- = \Omega_+$.

For a three level EIT scheme the steady state population in the ground states varies as $\rho_{22}^{ss}/\rho_{11}^{ss} = |C_2|^2/|C_1|^2 \simeq |\Omega_p|^2/|\Omega_c|^2$. The Raman beams Ω_+ and Ω_- cause population transfer within the ground states via optical pumping thereby departing the system from ideal steady state EIT behavior. The ground state populations in steady state can be expressed as

$$\frac{|C_2|^2}{|C_1|^2} \simeq \frac{|\Omega_p|^2}{|\Omega_c|^2} + \frac{(\Delta_c^2 + \gamma_3^2)}{(\Delta_R^2 + \gamma_3^2)}\frac{|\Omega_-|^2}{|\Omega_c|^2} + \frac{(\Delta_R^2 + \gamma_3^2)}{(\Delta_p^2 + \gamma_3^2)}\frac{|\Omega_p|^2}{|\Omega_+|^2}. \tag{S.45}$$
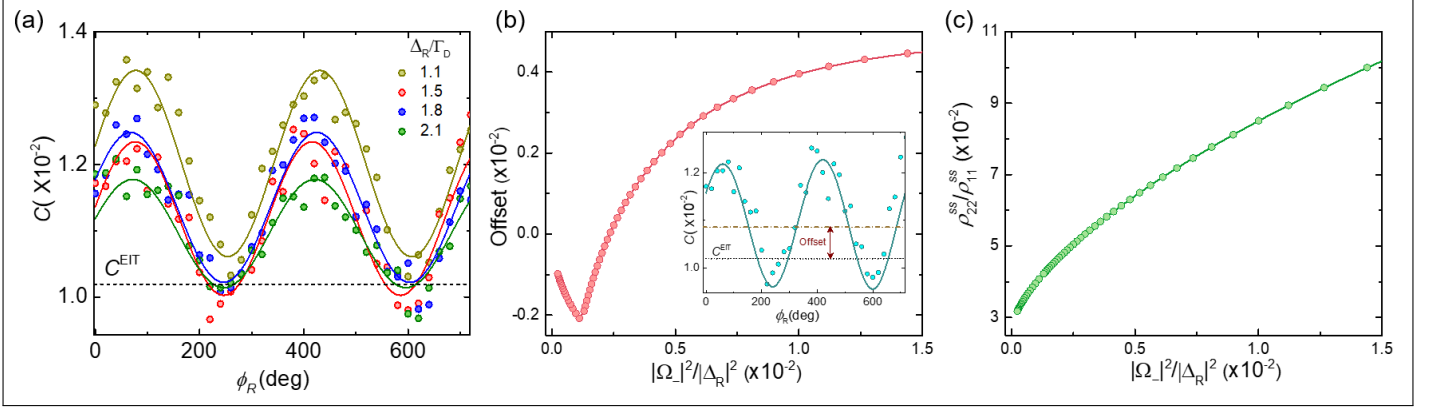
Fig. S.6. Asymmetry in C due to population redistribution by Raman beams. (a) Experimental plots for sinusoidal variation of C (circles) as a function of ϕ_R for varying Δ_R. Solid lines are the sine fits. The horizontal dashed line indicate C^{EIT}. Here $\Omega_c = 2.5 \times 10^{-1}\gamma_3$, $\Omega_p = 3.5 \times 10^{-3}\gamma_3$ and $|\Omega^+| = |\Omega^-| = 3.7 \times 10^{-1}\gamma_3$. (b) Offset in C with respect to C^{EIT} as a function of $|\Omega_-|^2/|\Delta_R|^2$. Inset indicates the definition of offset for $\Delta_R = 1.5\Gamma_D$. (c) Ratio of ground state populations as a function of $|\Omega_-|^2/|\Delta_R|^2$.

Here the last two terms are the correction terms due to optical pumping by the Raman beams, out of which the second term plays the dominant role. Therefore the population ratio $\rho_{22}^{ss}/\rho_{11}^{ss} \propto |\Omega_-|^2/|\Delta_R|^2$ as can be seen in Fig. S.6c. The offset is decided by the last two terms of equation (S.45), where we have considered that $\Omega_+ = \Omega_-$. Initially for small $|\Omega_-|^2/|\Delta_R|^2 = |\Omega_+|^2/|\Delta_R|^2$ the last term dominates and the offset is proportional to $|\Delta_R|^2/|\Omega_+|^2$ and when the second term dominates, offset is proportional to $|\Omega_-|^2/|\Delta_R|^2$, before reaching saturation.

REFERENCES

1. U. Schünemann, H. Engler, R. Grimm, M. Weidemüller, and M. Zielonkowski, "Simple scheme for tunable frequency offset locking of two lasers," Rev. Sci. Instruments **70**, 242–243 (1999).
2. D. A. Steck, "Rubidium 85 D line data, available online at http://steck.us/alkalidata (revision 2.1.6, 20 September 2013)," (2013).
3. D. Budker, *Atomic physics : an exploration through problems and solutions* (Second edition. Oxford ; New York : Oxford University Press, 2008). Previous ed.: 2004.; Includes bibliographical references (pages [491]-510) and index.
4. A. W. Laskar, N. Singh, A. Mukherjee, and S. Ghosh, "Interplay of classical and quantum dynamics in a thermal ensemble of atoms," New J. Phys. **18**, 053022 (2016).
5. A. S. Parkins, P. Marte, P. Zoller, and H. J. Kimble, "Synthesis of arbitrary quantum states via adiabatic transfer of zeeman coherence," Phys. Rev. Lett. **71**, 3095–3098 (1993).
6. T. Pellizzari, S. A. Gardiner, J. I. Cirac, and P. Zoller, "Decoherence, continuous observation, and quantum computing: A cavity qed model," Phys. Rev. Lett. **75**, 3788–3791 (1995).
7. J. I. Cirac, P. Zoller, H. J. Kimble, and H. Mabuchi, "Quantum state transfer and entanglement distribution among distant nodes in a quantum network," Phys. Rev. Lett. **78**, 3221–3224 (1997).
8. D. F. Phillips, A. Fleischhauer, A. Mair, R. L. Walsworth, and M. D. Lukin, "Storage of light in atomic vapor," Phys. Rev. Lett. **86**, 783–786 (2001).
9. M. Kozuma, D. Akamatsu, L. Deng, E. W. Hagley, and M. G. Payne, "Steep optical-wave group-velocity reduction and "storage" of light without on-resonance electromagnetically induced transparency," Phys. Rev. A **66**, 031801 (2002).
10. A. Streltsov, G. Adesso, and M. B. Plenio, "Colloquium: Quantum coherence as a resource," Rev. Mod. Phys. **89**, 041003 (2017).